Zeitschrift
für Physik C Particles
and Fields
© Springer-Verlag 1988

Jet reconstruction and jet properties at HERA

P.N. Burrows[1], G. Ingelman[2], E. Ros[2]

[1] Department of Nuclear Physics, University of Oxford, Oxford, OX1 3RH, UK
[2] Deutsches Elektronen-Synchrotron DESY, Notkestrasse 85, D-2000 Hamburg 52, Federal Republic of Germany

Abstract. We discuss jet reconstruction methods with respect to their suitability for ep collisions at HERA and study the expected properties of such jets. The results are based on complete event simulation using current models of jet evolution and hadronization in combination with experimentally tested jet algorithms. The effects of calorimeter resolution are illustrated by explicit simulation of the energy profile and fluctuations in a simplified, but realistic detector.

1 Introduction

The physics interest of studying hadron jets produced in ep collisions has several aspects. Firstly, it is closely related to many QCD phenomena and can thereby give information on parton processes as calculated in perturbation theory. Some such phenomena, e.g. high-$p_\perp$ particle production, occurrence of planar events and two-jet structure in the forward hemisphere have already been observed in fixed target muon scattering [1], but are expected to become much more pronounced and hence give more detailed QCD tests at ep collider energies [2]. However, other predicted phenomena, such as the angular energy flow asymmetry and the azimuthal asymmetries, which cannot be observed at present energies due to effects in the non-perturbative hadronization process [3] should finally be clearly observed at HERA. The increased phase space for parton radiation should lead to a larger fraction of *resolvable* multijet events which can be used for studies of gluon emission properties and α_s measurements from e.g., ratios of jet multiplicities. Secondly, jets in an ep collider are complementary to those produced in e^+e^- annihilation and hadron–hadron scattering in that they provide an additional test of jet universality; models for perturbative jet evolution and non-perturbative hadronization can thus be tested in another interaction and in the

kinematic domain of large spacelike momentum transfers. Thirdly, new heavy states decaying into quarks (and leptons) may be observable as resonances in invariant mass combinations of jets.

Before these physics topics can be realistically studied there are, however, a number of problems that have to be investigated and satisfactorily solved. Jets are measured experimentally either as groups of nearby particles identified in a tracking chamber or as associated clusters of energy in a calorimeter. In order that comparison between the measured, and theoretically predicted, jet properties can be realistically made, a jet finding algorithm suited to both should be used. An estimate of expected jet properties is, of course, of interest for designing experiments in the first place: the flow of energy and particles within the jet is important for both calorimetry and the ability to perform tracking in a jet environment.

A particular problem for ep colliders is the very unequal energies of the beams, e.g. 30 GeV electrons on 820 GeV protons at HERA, since this leads to a strong boost of the hadron system along the proton direction such that most hadrons appear in a rather small angular region and jets are thus less well separated in terms of laboratory angle. In the CM frame of the hadronic system, which is theoretically more convenient, one has a situation in between the 'clean' events in e^+e^- annihilation and that in 'messy' $p\bar{p}$ collisions, but transforming to this frame involves experimental uncertainties; the kinematics and particle masses need to be known.

We address these issues below. Current theoretical models for jets are briefly reviewed in Sect. 2 and the jet reconstruction methods discussed in Sect. 3. The jet properties are given in Sect. 4 and their relation to underlying parton clusters are discussed in Sect. 5. An estimate of how well the jet properties can be measured, using as an example information from a realistic calorimeter simulation, is given in Section 6 and we end with the main conclusions.

2 Jet models

Current state-of-the-art jet models (see e.g. [4] and references therein) are based on two main ingredients; perturbative QCD theory at the parton level and phenomenological models for the nonperturbative hadronization process. Exact matrix elements to leading and next-to-leading order in QCD have been used to give the production properties of jets, but have been shown to be inadequate for describing multijet events in e^+e^- annihilation [5,6] and internal jet properties of high-$p_\perp$ jets at the CERN $p\bar{p}$ collider [7]. The discrepancies are characteristic of higher order corrections and can be well accounted for by multiple gluon emission as treated in the parton shower approach. The basic idea here is that partons emerging from a large momentum transfer process can be off their mass shell and thus emit bremsstrahlung partons (mostly gluons) leading to a shower or cascade evolution at the parton level. Each emission is described by first order QCD in the leading logarithm approximation giving an iterative process, suitable for Monte Carlo simulation, which is terminated when the momentum transfer in the branching becomes small and hence makes perturbation theory unreliable. This is regulated by the virtuality cutoff parameter, t_{cut}, which together with Λ_{QCD} controls the amount of bremsstrahlung emitted. For the transition of these partons into hadrons one of a few alternative nonperturbative models has to be employed ([4,8,9]). The Lund string model [8] is particularly suitable since it provides a desirable stability [9,10] of the final hadron properties with respect to variations of the arbitrary t_{cut} parameter.

The Monte Carlo model [11] we use to simulate complete events in deep inelastic ep scattering is based on the electroweak cross-sections in the standard model (see e.g. [12]) with structure function parametrizations from [13]. For the treatment of QCD effects in the final hadronic system different possibilities are available [2]. The pure quark-parton model (QPM), without any perturbative QCD included, is too naive for our purpose of predicting realistic jet properties and is therefore not considered in this study. Also, the model based on exact QCD matrix elements, which are only available to order α_s [14,15], is expected to be insufficient at HERA energies, but we include it as an alternative to be compared with the parton cascade model (PC) in order to demonstrate the effects arising from the additional gluon emission.

The basic process $\gamma^* + q \to q$ is in first order QCD supplemented by gluon radiation and boson-gluon fusion, $\gamma^* + q \to q + g$ and $\gamma^* + g \to q + \bar{q}$. (The virtual photon may here also symbolize a general electroweak exchange of W and γ/Z bosons.) The matrix elements [14,15] have the usual soft and collinear divergences, which are avoided by requiring a minimum invariant mass m_{cut} between any pair of final partons (with the target remnant system counted as one parton). In contrast to the exact matrix elements, the parton

shower approach takes higher orders into account but does involve approximations, e.g. neglecting various interference effects. There is an arbitrary separation of an initial and final state cascade for radiation from the incoming and scattered quark, respectively. Both are treated by iteration of the three basic branchings $q \to qg$, $g \to gg$ and $g \to q\bar{q}$, as described by the Altarelli-Parisi equations [16]. The final state shower approach is well developed, with soft gluon interference effects taken into account [17], leading to a good agreement with the e^+e^- annihilation data at PETRA/PEP energies [18]. We are here using the algorithm in [19,20]. Although the initial state shower algorithms are less mature they have proven phenomenologically relevant for high-$p_\perp$ $p\bar{p}$ collider events. The backwards evolution scheme of [21,22] has been used in this study. The initial state radiation contributes less gluon emission than the final state one due to phase space differences and a suppression from structure function constraints on the incoming quark. It has therefore smaller influence on the hadronic final state [2] and is hence of less importance for our study. The lower cutoff for both cascades is chosen as $t_{cut} = 1\,\text{GeV}^2$ in accordance with e^+e^- phenomenology. The choice of scale for the maximum virtuality of the partons in the cascade is somewhat uncertain, but we follow [2] and choose the invariant mass-squared, $W^2 \equiv (q + P)^2 = Q^2(1 - x/x) + m_p^2$, of the hadronic system. This is in accordance with the observation [1] that transverse momentum effects (in the hadronic CM frame) depend essentially on W^2 as expected from the first order QCD matrix elements where $\langle p_\perp^2 \rangle \propto W^2$ [14]. Consequently jet properties will be given below as a function of W^2 rather than Q^2.

Once the parton configuration has been specified, by matrix elements or parton showers, the hadronization can be described by a phenomenological fragmentation model; we use the Lund string model [8]. In the simplest case, where a valence quark is scattered without gluon emission, a string is stretched between this quark and the target remnant diquark. In more complicated cases there may be one or more strings, each corresponding to a colour singlet subsystem and being stretched between a quark end and an antiquark or diquark one, with gluons appearing as energy and momentum carrying kinks on these strings. For both first order matrix elements and parton showers, the way the strings should be stretched between the scattered partons (i.e. their colour ordering) is unambiguous. The treatment of the hadron remnant system (which is usually not unique) is discussed in [2,11], but is not important for this study since most of the target jet will be lost down the beam pipe and any remaining fragments outside can be isolated.

3 Jet reconstruction

The structure of jets in the hadronic final state is most naturally studied in the hadronic CM frame,

i.e. the centre-of-mass of the exchanged boson and the beam proton, where the scattered quark is (nearly) back-to-back with the target remnant jet. Additional jets from gluon radiation can here also be more separated in angle and hence easier to study. However, the actual measurements are performed in the laboratory frame which differs by a typically large boost along the proton beam axis, giving the events a 'forward-boosted' character. This presents some problems for jet analysis since the widths, separation and relative energies of jets, become influenced by this boost making the interpretation of these properties in terms of the underlying QCD processes more difficult. For example, a narrow high energy jet which is very forward in the lab frame may actually be a wide low energy jet rather centrally placed in the hadronic CM frame, which has simply gained energy and been narrowed by the boost. This effect can, in principle, be unfolded once the kinematics, e.g. x and Q^2, of the event have been measured and the boost calculated, but some problems still remain in assigning masses to the particles or, more seriously, to calorimeter cell 4-vectors (including neutral particles).

Jets in different regions of the laboratory phase space corresponding to the forward, central and backward parts of the detector will typically correspond to different kinematics, i.e. different boosts, and thus have different widths in terms of lab angle. A realistic experimental jet-finding algorithm for the lab frame must take this into account. This immediately rules out jet algorithms of the type which maximise energy deposits within a cone of certain fixed half-angular width δ; a δ suitable for jets in the central region, say 30^0, would completely swallow up the entire forward region and not be able to resolve any multijet structure there. One could take this into account by allowing δ to be a function of the polar angle θ, but the functional form would have to be postulated. One possibility is the UA1 type of algorithm, which searches for deposits of energy within a cone of width $\Delta R = \sqrt{\Delta\eta^2 + \Delta\phi^2}$ in the pseudorapidity-azimuthal angle space divided into cells of specified area $\Delta\eta_0 \times \Delta\phi_0$. This algorithm lends itself naturally to jet reconstruction using calorimeter information, in particular if the calorimeter segmentation matches the grid size used. Since ϕ is invariant under longitudinal boosts and a fixed $\Delta\eta$ corresponds to smaller angles in the problematic forward proton direction, this kind of algorithm is in fact quite useful also for ep collider events. One still has the freedom of summing either transverse energies (as in the $p\bar{p}$ case) or total energies which will give different results in the forward region and be sensitive to the boosts discussed above. For a calorimeter with non-projective geometry (see Appendix) the choice of grid size is furthermore not straightforward since the separation of nearby cell 4-vectors, obtained from the energy deposited in a calorimeter cell and its position relative to the interaction point, will vary from one part of the detector to another. In

order not to lose information in this case, it is essential that the grid size, $\Delta\eta_0\Delta\phi_0$, is smaller than the finest resolution achievable from the calorimeter cell 4-vectors. We have found that such an algorithm would work in the HERA lab frame, though we do not present any results here.

For our study we choose instead a cluster algorithm which has theoretical advantages and which has also been used successfully for multijet studies at PETRA [5,6]. The invariant mass-squared m_{ij}^2 is formed for all particles i, j in an event and the pair with the smallest mass is combined into a pseudoparticle by adding the momentum four-vectors. This process is repeated until *all* remaining pairs of particles or pseudoparticles have invariant masses which satisfy:

$$m_{ij}^2 > m_c^2 = y_c W^2 \quad \text{for all} \quad i, j.$$

The resulting number of (pseudo) particles is called the jet multiplicity of the event and their 4-vectors are the desired jet vectors with respect to which the internal jet properties are obtained from all particles assigned to the jet. Such an algorithm has many attractive features, in particular:

• It is Lorentz invariant: the same particles will be combined into the same jets no matter in which frame the algorithm is used.*

• It is equally suited to jet reconstruction from *either* particles measured in a tracking chamber *or* from four-vectors assigned to deposits of energy in calorimeter cells.

• It contains only one arbitrary parameter y_c, whose value can be chosen from experience at PETRA.

• It provides 'infra-red stability': the y_c parameter corresponds to the usual cutoff for soft and collinear divergences when calculating matrix elements in QCD at the parton level and thus facilitates easy comparison of theoretical 'parton jets' and experimentally reconstructed jets.

The results we present can also be compared with measured jet properties in e^+e^- annihilation [5,6] and other predictions at future e^+e^- and $p\bar{p}$ colliders [24,25].

In accordance with PETRA studies we choose $y_c = 0.04$ at $W = 35\,\text{GeV}$ and fix the minimum invariant-mass-squared for pairs of jets at:

$$m_c^2 = 0.04 \times 35^2 = 49(\text{GeV/c}^2)^2.$$

(Some results will also be shown for $y_c = 0.08$ in Sect. 5). Note that we keep the jet mass-resolution fixed since this corresponds to a constant ability to resolve jets with a given detector, independent of W. Keeping y_c fixed is unphysical since it implies a jet resolution capability which decreases as W increases.

---

* Up to particle mass effects. Note, however, that the properties of these jets will vary from frame to frame

4 Jet properties

Monte Carlo [11] simulated ep collision events at the nominal HERA energy are used to investigate the expected properties of jets. In particular we examine the evolution of these jet properties with increasing energy scale, i.e. as a function of W^2, which was taken to define the virtuality scale in the parton cascade approach and which is also the main variable for $p_\perp$ effects (in the hadronic CM) according to the first order QCD matrix elements [14]. In the lab frame, however, the $p_\perp$ of the scattered quark, which is given by $p_\perp^2 = Q^2(1 - y)$, is a kinematical effect and hence not so interesting for jet evolution properties in the QCD language. We thus select values of W_0^2 of 10^3, 10^4, 5×10^4 GeV^2 and generate complete neutral current events, allowing the kinematical variables x, Q^2 to vary to give W^2 within the range $0.9 W_0^2 < W^2 < 1.1 W_0^2$. In this way 'natural' values of x, Q^2 are chosen according to the differential cross-section, and there is no artificial biasing of the resulting jet properties by the choice of atypical values to give the required W_0^2. However, we do force the kinematics to be measurable experimentally by imposing the cuts [26]:

for $W_0^2 = 10^3$ GeV^2: $x > 10^{-2}$ $y > 0.03$ $Q^2 > 100$ GeV^2

for $W_0^2 \geq 10^4$ GeV^2: $x > 10^{-4}$ $y > 0.1$ $Q^2 > 10$ GeV.

In the first case x, Q^2 can be determined from the

Table 1. Kinematics

W_0^2(GeV^2)	10^3	10^4	5×10^4
$\langle x \rangle$	0.7	0.007	0.002
$\langle Q^2 \rangle$ (GeV^2)	2500	70	100
N^0 of events/year @ 100 pb^{-1}	3	120k	150k

Table 2. Event statistics ($2.3° < \theta_{\text{particle}}^{\text{lab}} < 176.5°$)

W^2(GeV^2)	10^3	10^4	5×10^4
		$O(\alpha_s)$	
$\langle n \rangle$	15.7	25.5	30.9
$\langle n/\text{jet} \rangle$	9.9	11.9	12.6
		Parton cascade	
$\langle n \rangle$	16.1	28.1	42.3
$\langle n_{\text{ch}} \rangle$	7.5	13.1	19.8
$\langle n/\text{jet} \rangle$	10.3	12.5	13.5
$\langle n_{\pi^+} \rangle$	3.4	5.6	8.3
$\langle n_{\pi^-} \rangle$	3.0	5.5	8.3
$\langle n_{K^+} \rangle$	0.35	0.59	0.95
$\langle n_{K^-} \rangle$	0.28	0.58	0.92
$\langle n_p \rangle$	0.24	0.38	0.59
$\langle n_\gamma \rangle$	8.0	13.7	20.9
$\langle n_{K_L^0} \rangle$	0.30	0.56	0.86
$\langle n_{e\pm} \rangle$	0.05	0.09	8.14

hadronic system using the Jacquet–Blondel method [27] and in the second directly from the energy and direction of the scattered electron. The resulting kinematics is illustrated in Table 1. The case $W^2 = 10^3$ GeV^2 roughly corresponds to the CM energy at which the bulk of PETRA data was obtained and is therefore included only for comparison purposes; such events comprise a tiny fraction of the cross-section at HERA. The two higher W^2 ranges are however expected to be regions of abundant jet production, as can be seen from Table 1. It should be noted that the Q^2's for production of such typical jets are very modest, around 100 GeV^2, and it is also amusing that the *lowest* W^2 range corresponds to events with the *highest* Q^2, a consequence of the dominance of the cross-section at small x and the larger cut in x in this case.

Results are presented for the two treatments of the perturbative QCD processes as discussed in Sect. 2.:

(i) the first order exact matrix element ('$O(\alpha_s)$'), which is not expected to reproduce well the correct features of multijet events, as the corresponding $O(\alpha_s^2)$ matrix element for e^+e^- has already been shown to be deficient at PETRA energies [5,6].

(ii) a leading logarithm Parton Cascade ('PC') approximation for parton radiation in the initial and final states. A similar QCD approach for e^+e^- annihilation has been shown to reproduce extremely well the rates of multijet events observed at PETRA [5,6,28].

In both cases the Lund string model [8] is used for the non-perturbative hadronization process. The scattered lepton is always removed from the simulated

Table 3. Jet properties (hadronic CM frame)

W^2(GeV^2)	$O(\alpha_s)$			Parton cascade		
	10^3	10^4	5×10^4	10^3	10^4	5×10^4
$\langle n_{\text{jet}}/ev \rangle$	1.6	2.1	2.5	1.6	2.2	3.2
$\langle n_{\text{jet}}^{\text{quark}}/ev \rangle$	0.95	1.4	1.4	0.8	1.0	1.2
$\langle n_{\text{jet}}^{\text{gluon}}/ev \rangle$	0.24	0.17	0.11	0.33	0.79	1.2
$\langle n/\text{jet} \rangle$	9.9	11.9	12.6	10.3	12.5	13.5
$\langle E_{\text{jet}} \rangle$ (GeV)	11.0	24.7	43.8	11.1	24.0	36.6
$\langle E_{\text{jet}}^{\text{quark}} \rangle$ (GeV)	15.4	33.7	69.9	15.0	35.4	55.4
$\langle E_{\text{jet}}^{\text{gluon}} \rangle$ (GeV)	7.4	14.3	27.7	11.4	19.3	32.4
$\theta_{\text{jet}}^{\text{CM}} < 120°$:						
$\langle n_{\text{jet}}/ev \rangle$	1.3	1.8	1.6	1.3	2.0	2.3
$\langle n_{\text{jet}}^{\text{quark}}/ev \rangle$	0.95	1.4	1.3	0.81	0.98	1.1
$\langle n_{\text{jet}}^{\text{gluon}}/ev \rangle$	0.18	0.14	0.08	0.30	0.73	1.0
$\langle n/\text{jet} \rangle$	10.7	12.7	13.7	11.2	13.2	14.4
$\langle E_{\text{jet}} \rangle$ (GeV)	12.8	29.0	64.5	12.7	26.9	47.2
$\langle E_{\text{jet}}^{\text{quark}} \rangle$ (GeV)	15.4	35.3	74.7	15.0	36.6	62.7
$\langle z_{\text{particle}}^{\text{quark}} \rangle$	0.12	0.10	0.093	0.12	0.097	0.093
$\langle E_{\text{jet}}^{\text{gluon}} \rangle$ (GeV)	8.6	15.9	34.8	12.3	20.7	38.2
$\langle z_{\text{particle}}^{\text{gluon}} \rangle$	0.12	0.11	0.092	0.10	0.094	0.085

event in order that the following results refer to the hadronic system only.

The increase of the stable particle multiplicity with increasing W^2, due to the increasing gluon emission, is shown in Fig. 1 for the PC. Note that the total particle multiplicity is not a meaningful quantity from an experimental point of view, as a large number of particles associated with the hadronization of the proton fragment are swept down the beam pipe and are not detected. For all results we have therefore imposed a 'beam pipe acceptance' for particles of $2.3° < \theta^{lab}_{particle} < 176.5°$, where $\theta^{lab}_{particle}$ is the angle with respect to the initial proton direction, which corresponds to the angular coverage of the ZEUS calorimeter (see Appendix). Reasonably small variations in this cut do not significantly affect our results on jet properties. The resulting particle multiplicity therefore corresponds to that which would be contained 'within a HERA detector'. Values of the mean total and charged multiplicities for the PC and $O(\alpha_s)$ are shown in Table 2, together with the different
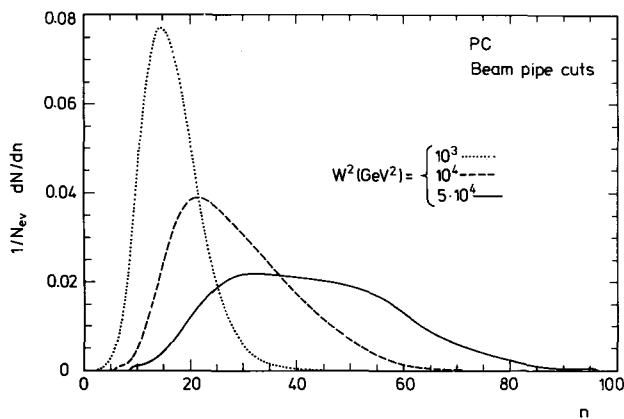
Fig. 1. The stable particle multiplicity distribution for the parton cascade with the beam pipe cuts $2.3° < \theta^{lab}_{particle} < 176.5°$. $W^2 = 10^3$ (dotted), 10^4 (dashed), 5×10^4 (solid) GeV^2

Fig. 3 a, b. The jet angular distribution for the parton cascade in: a the hadronic CM frame, with respect to the axis given by the direction of the exchanged virtual boson, b in the lab frame, with respect to the initial proton direction. $W^2 = 10^3$ (dotted), 10^4 (dashed), 5×10^4 (solid) GeV^2
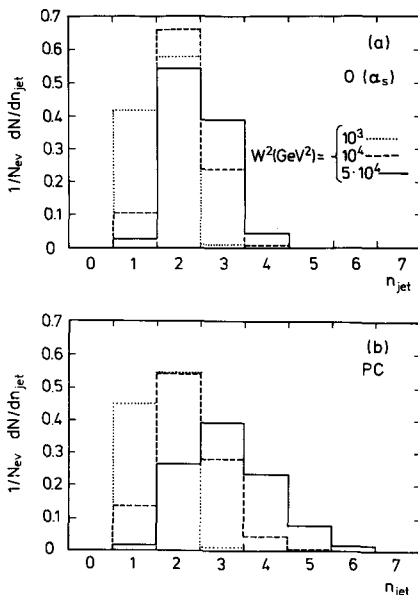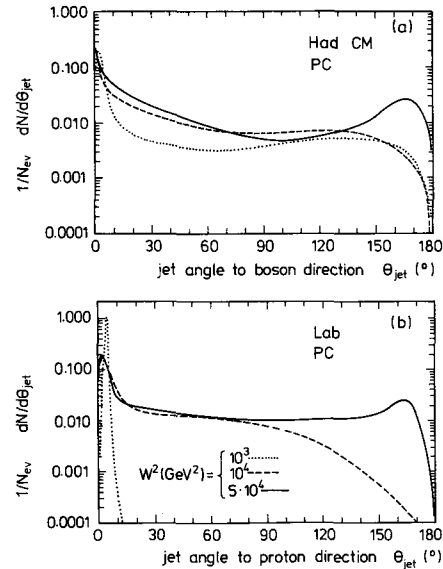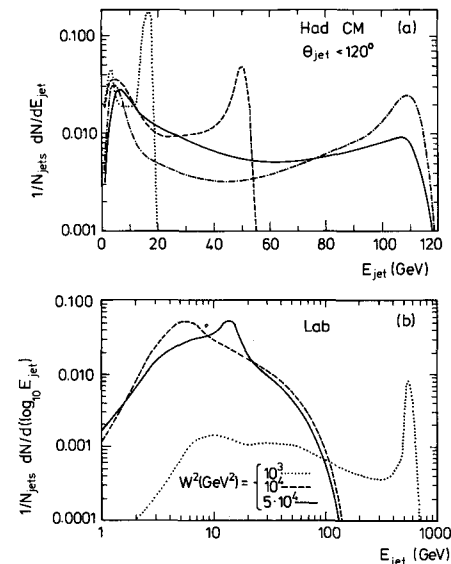

Fig. 2 a, b. The number of reconstructed jets per event: a for the $O(\alpha_s)$ matrix element, b for the parton cascade. $W^2 = 10^3$ (dotted), 10^4 (dashed), 5×10^4 (solid) GeV^2

Fig. 4 a, b. The jet energy distribution for the parton cascade in: a the hadronic CM frame, with $\theta^{CM}_{jet} < 120°$, b in the lab frame. $W^2 = 10^3$ (dotted), 10^4 (dashed), 5×10^4 (solid) GeV^2. In (a) an additional curve (dash-dotted) is shown for the $O(\alpha_s)$ generator at $W^2 = 5 \times 10^4$

particle fractions. As expected, the $O(\alpha_s)$ gives a slower increase in multiplicity with W^2 and much narrower multiplicity distributions (not shown) due to the absence of higher order parton radiation processes.

The number of jets per event, reconstructed as described in Sect. 3, is shown in Fig. 2, their angular and energy distributions in Figs. 3, 4 respectively, with some numerical values in Table 3. Only particles within the beam pipe acceptance described above are used for the jet reconstruction. The PC gives a much richer jet structure than the $O(\alpha_s)$, as can be seen from the larger number of jets (Fig. 2), most of which are of lower energy (Fig. 4a). The number of jets reconstructed clearly depends on the value chosen for the mass resolution parameter m_c^2. The fact that the $O(\alpha_s)$ gives more than two jets at higher W^2, when at most two-parton states are allowed (neglecting the proton remnant) suggests that the 'PETRA value' $y_c = 0.04$ at $W = 35$ GeV may be too small for the range of W^2 spanned by HERA. Some results are also presented for the larger value of 0.08 (Section 6).

Figure 3b shows that in the lab frame jets are mostly at small angles to the beam proton, due to the combined effect of the boost and the gluon radiation. For $W^2 = 5 \times 10^4$ GeV^2 there is even an excess in the number of jets close to the proton direction in the hadronic CM frame, $\theta_{jet}^{CM} = 180°$ in Fig. 3a, which are in general reconstructed from target fragmentation products with sufficient transverse momentum to have

leaked out of the beam pipe, and are hence usually not of interest. Due to the losses in the beam pipe such jets are heavily biased and hence of low multiplicity and with a very hard fragmentation spectrum of
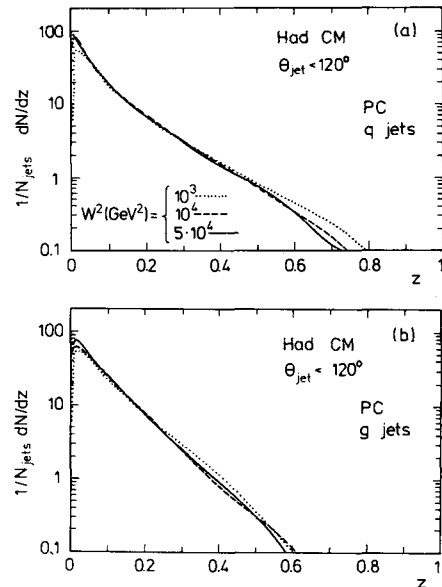

Fig. 5 a, b. The fragmentation function for charged particles in jets in the hadronic CM frame ($\theta_{jet}^{CM} < 120°$) for the parton cascade. The scaled energy variable is $z = E_{particle}/E_{jet}$: **a** for quark jets, **b** for gluon jets. $W^2 = 10^3$ (dotted), 10^4 (dashed), 5×10^4 (solid) GeV^2
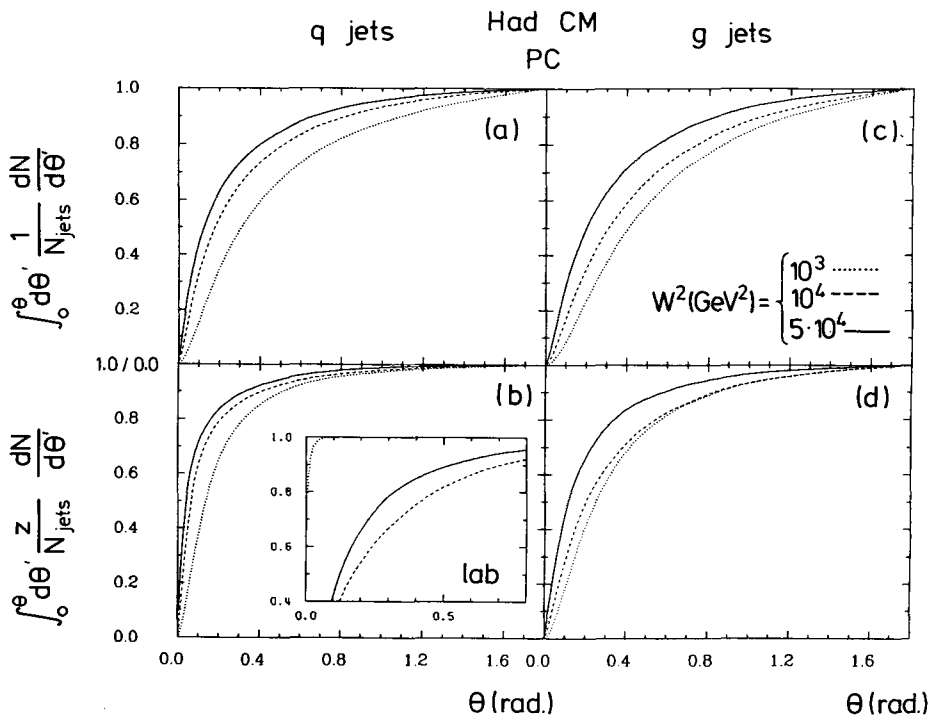

Fig. 6 a-d. The particle and energy flows for quark jets **a, b** respectively and gluon jets **c, d** respectively, in the hadronic CM frame for the parton cascade ($\theta_{jet}^{CM} < 120°$). The insert in **b** shows the energy flow for quark jets in the lab frame. $W^2 = 10^3$ (dotted), 10^4 (dashed), 5×10^4 (solid) GeV^2
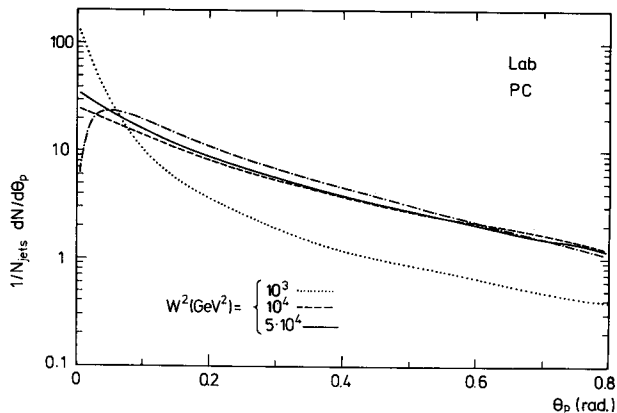
Fig. 7. The angle between nearest-neighbour charged particles in jets, projected onto the plane transverse to the initial particle beams, in the lab frame for the parton cascade. $W^2 = 10^3$ (dotted), 10^4 (dashed), 5×10^4 (solid) GeV^2. An additional curve (dash-dotted) is shown for the *unprojected* angle for $W^2 = 5 \times 10^4$

the same W^2 the energy flow is much narrower than the particle flow, and both narrow as W^2 increases. Similar trends are seen for the $O(\alpha_s)$ model (not shown). The insert in Fig. 6b illustrates the confusion which occurs in the lab frame, where the jets produced at the *lowest* W^2 are the *narrowest* due to the large boost from the hadronic CM to the lab. The jet width is also reflected in the angular separation between nearest neighbour charged particles, shown for the PC in the lab in Fig. 7. The angle in space between such particle pairs is of course larger than the angle in projection upon the plane transverse to the incident particle beams, though the latter is of more interest for the ability to reconstruct charged particles in a tracking chamber.

5 Relationship between jets and partons

The relation between the observed hadronic jets and the underlying parton level processes is important for the theoretical interpretation of jet phenomena. In fixed, low-order perturbation theory only a few hard partons are produced. With the inclusion of the higher orders in the parton cascade approach many-parton final states will occur frequently and, in particular, the multiplicity of softer (bremsstrahlung) gluons increases. In this case it is not meaningful to consider individual softer partons, since they are not usually of interest and their effect on the final state cannot be disentangled experimentally. Also the hard partons cannot be directly identified with the observed jets, since the latter usually depend on more than one parton and it is, therefore, collections of partons that should be compared with the hadron jets. For this purpose we apply the same jet/cluster finding algorithm to the final parton state of the Monte Carlo generated events to obtain such 'parton clusters', which can then be compared with the hadron jets obtained after hadronization of the same events. The parton clusters (c) are then associated with the hadron jets (j) by finding the pairs with maximum dot products of 3-vectors in the hadronic CM frame, i.e. $(\mathbf{p}_j \cdot \mathbf{p}_c)/(|\mathbf{p}_j| \cdot |\mathbf{p}_c|)$.

We made use of this method in Section 4 when assigning quark or gluon flavour to a hadron jet: working in the hadronic CM frame, the parton clusters are found and flagged as either 'quark' or 'gluon' according as to whether the most energetic parton in the cluster is a quark or gluon respectively, provided that the energy of the second-most energetic parton does not exceed 70% of the first one, giving an ambiguous case where no jet flavour is assigned. Note that whilst the particle clustering into jets is Lorentz invariant, the flavour assignment is not, for the relative energies of partons change from frame to frame.

In Fig. 8 we show typical results of such a comparison of parton clusters and hadron jets for HERA events at $W^2 = 10^4$ GeV^2. The distribution of the number of reconstructed parton clusters per event and
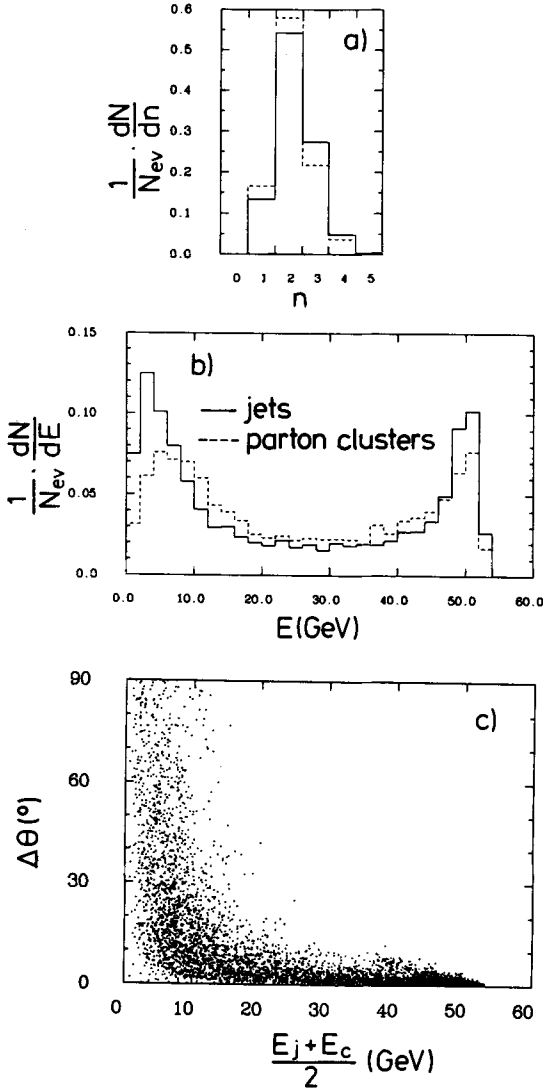
particles. In order not to bias our study of the QCD evolution of the jet properties, we exclude such jets by requiring the jet angle to be $< 120°$ in the hadronic CM for some figures. The effect of this cut on the global jet properties is clearly seen in Table 3.

The mentioned mixup of jet energies due to the boost is well illustrated in Fig. 4 where the jets in the $W^2 = 10^3$ GeV^2 sample have the *lowest* energy in the hadronic CM frame, but the *highest* energy in the lab frame. More importantly, Fig. 4a shows that in the hadronic CM frame, for each W^2, there are a large number of high energy jets for which no hard parton radiation leading to resolvable substructure has occurred, in particular at lower W^2 where a peak at the maximum jet energy is clearly seen. This peak is reduced at larger W^2, where instead a relatively larger number of lower energy jets corresponding to resolved parton bremsstrahlung is observed. The PC distribution is much more smeared than that for the $O(\alpha_s)$ model (compare the full and dash-dotted curves in Fig. 4a) as a result of the more prolific gluon emission in the former.

Figure 5 shows the fragmentation function for charged particles in quark and gluon jets for the PC, where the jet flavour was assigned as described in Section 5. As W^2 increases, the population of the low z region, which contains the bulk of the particle multiplicity, increases, so that the fragmentation function softens due to the increasing amount of gluon emission. There are fewer hard particles (e.g. $z > 0.5$) in the gluon jet sample even though these jets are of lower energy than the quark jets (Table 3). The $O(\alpha_s)$ results show the same trends and are not plotted, though it can be seen from the mean values of z given in Table 3 that there are in general, as expected, more hard particles than for the PC model.

The particle and energy flows transverse to the jet axis are shown for the PC in the hadronic CM for quark and gluon jets in Fig. 6. For jets produced at

Fig. 8 a-c. Comparison of **a** multiplicity and **b** energy of parton clusters (dashed) and hadronic jets (full) as reconstructed with the same algorithm from HERA events at $W^2 = 10^4 \, \text{GeV}^2$. **c** Space angle, $\Delta\theta$, between cluster and jet axes in the hadronic CM frame, versus cluster/jet energy

that of jets agree well, Fig. 8a. On average, fluctuations due to hadronization yield more jets than parton clusters: $\langle n_j \rangle = 2.25$, $\langle n_c \rangle = 2.13$. This good agreement is also seen in the jet/cluster energy distribution (Fig. 8b), there being slightly more lower energy jets than clusters: $\langle E_j \rangle \simeq 24 \, \text{GeV}$, $\langle E_c \rangle \simeq 25 \, \text{GeV}$.

In averaging over many events, therefore, the parton clusters and jets have very similar properties. To establish that fluctuations on a jet-by-jet basis are small, we show in Fig. 8c a scatter plot of the space angle, $\Delta\theta$, between each cluster and its associated jet (see above) in the hadronic CM frame, as a function of the energy $(E_j + E_c)/2$. Figure 8c contains all associated cluster/jet pairs; the fraction of events in which the numbers of clusters and jets do not match

is small: $\sim 6\%$ have one more cluster than jets and $\sim 5\%$ have one more jet than clusters. (Note that the very dense region, $E > 20 \, \text{GeV}$, which cannot be properly resolved, contains the vast majority of the pairs and the high $\Delta\theta$-tail at small energies should not be over-emphasised.) We find that:

(i) most jets have axes within a few degrees of their parton cluster

(ii) the jets at large angle to their associated cluster are typically of rather low energy, and hence sensitive to fluctuations caused by the hadronization.

We conclude that a meaningful association can be made between the jets in our study and the corresponding underlying parton level processes, not only on a statistical, event-averaged basis, but also event-by-event.

6 Jet reconstruction from a calorimeter

In order to study how the above jet properties may be affected by the various effects that arise in an experiment we have taken, as an example, jet reconstruction from a calorimeter. The geometry of the ZEUS detector and its response to electromagnetic and hadronic energy deposits was simulated in a simplified way. The ZEUS calorimeter is of the uranium-scintillator sandwich type and covers the whole solid angle except for a small region around the beam pipe. The expected energy resolution is $\sigma/E = 35\%/\sqrt{E}$ for hadrons and $\sigma/E = 15\%/\sqrt{E}$ for electrons and photons. The granularity is given by about 1400 towers with $20 \times 20 \, \text{cm}^2$ front size. An important fact is that the geometry is non-projective. For more details about the structure of the calorimeter and the simulation of its performance, we refer to the appendix.

The Monte Carlo generated events, with the scattered lepton removed, are thus passed through this detector simulation program resulting in energy deposits in the calorimeter cells which are treated as massless pseudoparticles of energy equal to the cell energy and direction pointing from the interaction point to the geometrical centre of the cells. The jet finding algorithm is then applied to these pseudo-particles and the resulting jet properties compared with the genuine jets obtained without calorimeter smearing effects.

Figure 9 shows the reconstructed jet multiplicity before and after calorimeter simulation and for two values of the basic jet resolution parameter, $y_c = 0.04$ and 0.08. The lost resolution due to finite calorimeter segmentation favours the larger y_c, which is then used for the comparison of the more detailed jet properties shown in Fig. 10. With this y_c there is quite good agreement between the jet properties obtained with and without calorimeter simulation, whereas for $y_c = 0.04$ large differences are observed. The net effect of leakage and fluctuations in response from the calori-
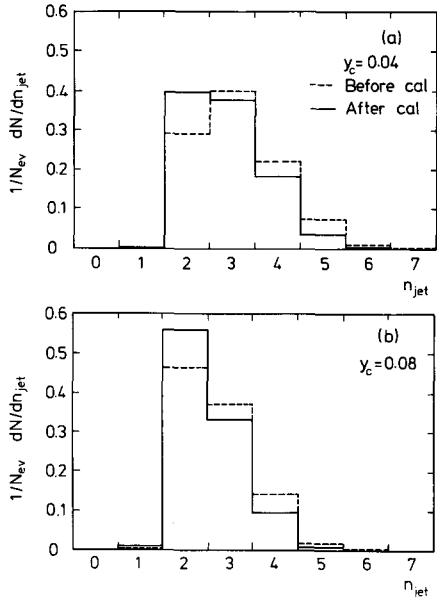
Fig. 9 a, b. The number of reconstructed jets per event for **a** $y_c = 0.04$, **b** $y_c = 0.08$, for the parton cascade at $W^2 = 5 \times 10^4$, before (dashed) and after (solid) ZEUS calorimeter simulation
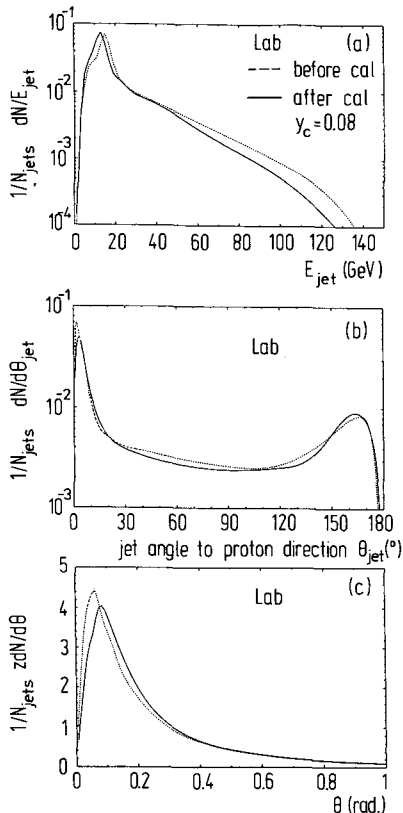

Fig. 10 a-c. The jet energy distribution **a**, the jet angular distribution with respect to the initial proton direction **b** and the energy flow transverse to the jet axis **c**, in the lab frame for the parton cascade at $W^2 = 5 \times 10^4$, before (dashed) and after (solid) ZEUS calorimeter simulation

meter is that jets are reconstructed with slightly lower energy than their 'true' value (Fig. 10a). There is good agreement in the jet angular distribution before and after calorimeter (Fig. 10b), which shows that overall shifts due to the non-projective geometry are small, and that shower spreading in the calorimeter does not, on average, significantly affect the direction of the reconstructed jet axis. As expected, however, this shower development transverse to the jet axis results in a slightly wider energy flow (Fig. 10c).

Bearing in mind the approximations used in our simulation, it is promising that such good agreement between the 'true' and calorimeter-determined jet properties is obtained. It is likely that an even better agreement could be achieved by tuning y_c to some optimal value to compliment the calorimeter response: effects due to the segmentation, leakage between cells, shower fluctuations etc. can be minimised by choosing a lower jet resolution criterion (higher y_c), though an upper limit on y_c is provided by the requirement to resolve spatially well-separated showers. Another possibility which might improve agreement is to normalise m_c^2 by the total energy measured in the calorimeter: $m_c^2 \to \propto m_c^2 \times E_{vis}^2$, thereby taking into account energy leakage and fluctuations. Such fine tuning is clearly not appropriate for this study, given the simplified simulation used, but should be considered for the real calorimeters when they are in operation.

It thus seems realistic that the main jet properties presented in this paper can be readily measured at HERA. With the addition of particle tracking information, which we have not simulated, it should be possible to thoroughly explore most features of such hadronic jets.

7 Conclusions

Based on the phenomenological success of current state-of-the-art models for jet evolution and hadronization at present energies it is reasonable to extrapolate to higher energies in order to predict the expected jet properties. In fact, available data and theoretical considerations constrain the models quite considerably, leaving a rather limited range of possible variations. The jets at HERA will, furthermore, be in an energy region overlapping with that observed in $p\bar{p}$ collisions where a satisfactory agreement between data and models has been found, which naturally puts the predictions on a firmer ground. Nevertheless, there are differences in that ep collisions involve large space-like momentum transfers where the parton cascade approach has only recently been developed and not yet confronted with data. The necessity of this parton cascade evolution, in order to effectively take higher order emission into account, is clear from experiences in e^+e^- and $p\bar{p}$ phenomenology and is also found in this study to give significantly different results compared to the first order QCD matrix elements.

The predicted jet properties concerning longitudinal and transverse flows of particles and energy, and the differences between quark and gluon jets, are found to vary with energy basically as expected. We emphasise, however, that this is only clear in the hadronic CM frame, since the boost to the ep laboratory frame makes drastic changes to jet energies and angular measures. The former frame is thus preferred for phenomenological analyses. An experimentally tested jet finding algorithm with theoretically attractive features was used in order that the predicted jet properties correspond to the jets that will be observed. By a similar analysis of the multiparton final state (before hadronization) parton clusters were reconstructed and found to correspond closely to the hadronic jets, demonstrating the direct relation between the observable jets and the underlying parton level processes.

Detector effects were investigated by simulating the response of a simplified, but realistic, calorimeter and found to alter the observable jet properties only slightly. Thus we can conclude that the most important jet properties should be measurable in the planned experiments at HERA using realistic jet reconstruction methods.

Appendix: the calorimeter simulation

The ZEUS calorimeter [29] consists of 3 components (see Fig. 11):

- a forward calorimeter (FCAL) in the direction of the proton beam,
- a barrel calorimeter (BCAL) covering the angular region between $\theta = 36.7°$ and $\theta = 129.1°$,
- a rear calorimeter (RCAL) in the direction of the electron beam.

The depths of these 3 components are respectively 7, 5 and 4 interaction lengths. This calorimeter is hermetic except for the beam pipe hole (2.3° in the proton direction and 3.5° in the electron direction). Longitudinally the calorimeter is segmented into an electromagnetic section (EM) and 2 hadronic sections (HAD) except in the RCAL where there is only one hadronic section. In the transverse direction the calorimeter is segmented into $20 \times 20\,\mathrm{cm}^2$ towers which are further divided into $5 \times 20\,\mathrm{cm}^2$ strips in the EM sections. The towers in the FCAL and RCAL are nonprojective. In the BCAL the towers are projective in ϕ but not in θ except for the EM sections. The calorimeter is of the sandwich type, the layer structure conisting of 3.3 mm thick uranium plates and 2.6 mm thick scintillator plates. These thicknesses ensure that the calorimeter is compensating (equal response for electrons and hadrons). The measured energy resolutions for electrons and hadrons are respectively $\sigma/E = 15\%/\sqrt{E}$ and $\sigma/E = 35\%/\sqrt{E}$. The light produced in the scintillator is collected by photomultipliers via an optical system consisting in wave-
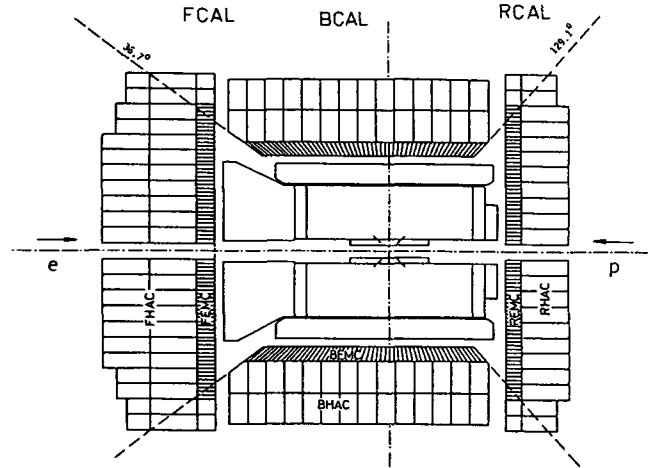

Fig. 11. Basic geometry of the ZEUS calorimeter showing the cell structure in the forward (FCAL), barrel (BCAL) and rear (RCAL) components

length shifter plates and light guides. There are approximately 1400 towers in the whole calorimeter.

The cell structure of the ZEUS calorimeter has been completely simulated with, however, the following simplifications:

- the strip segmentation of the EM sections has not been included,
- the EM sections of the BCAL have been made nonprojective,
- no cracks between the components have been included,
- some towers at the corners of the FCAL and BCAL which are absent in the real design have not been suppressed,
- the varying depth of FCAL and RCAL towers introduced in the real design has not been included.

These simplications do not alter the basic properties of the calorimeter in what concerns jet analysis or energy response in general. Some granularity and angular resolution power is however lost, especially for electrons where we underestimate the measuring accuracy.

For the shower generation in the calorimeter, the average profiles are simulated by the Monte Carlo method according to the energy and the type of particle hitting the calorimeter. The energy deposited in each cell is calculated for each event after summing up the energy deposited by all the 'stable' particles produced in the event $(e, \gamma, \pi, p, n, K)$. The longitudinal and transverse average shower profiles for electrons and photons were obtained by fitting Monte Carlo data produced with the help of the EGS generator [30]. The average profiles of hadronic showers were obtained by fitting the data collected for uranium test calorimeters [31]. The global energy fluctuation of each shower is simulated according to the measured values of the energy resolution mentioned before. In

this scheme for shower simulation the following simplification are made:

- the shower profiles are only average profiles and therefore no local fluctuations are taken into account,
- longitudinal and transverse profiles are considered uncorrelated,
- all hadrons are treated as pions and no account has been taken of the rest masses, which may be important for low momentum particles,
- it has been assumed that muons do not deposit any energy in the calorimeter,
- no dependence of the energy resolution with respect to the angle of incidence (of the particles to the calorimeter) has been considered,
- no instrumental effects due to nonuniformities or calibration errors have been considered. These effects introduce a constant term of typically 1 or 2% in the energy resolution.

The precise simulation of all these effects is needed for a very detailed analysis of the calorimeter response, but not required for our study of jet properties at this stage. For the jet reconstruction algorithms the energy of each cell is translated into a 'pseudoparticle' of zero rest mass, energy equal to the energy of the cell and direction pointing to the geometrical center of the cell.

References

1. J.J. Aubert et al. EMC Collab.: Phys. Lett. 95B (1980) 306; Phys. Lett. 100B (1981) 433; Phys. Lett. 130B (1983) 118; M. Arneodo et al. EMC Collab.: Phys. Lett. 149B (1984) 415; CERN-EP/87–112 (1987)
2. M. Bengtsson, G. Ingelman, T. Sjöstrand: DESY 87–097 (1987), Nucl. Phys. B301 (1988) 554
3. G. Ingelman, B. Andersson, G. Gustafson, T. Sjöstrand: Nucl. Phys. B206 (1982) 239
4. G. Ingelman: DESY 87–145 (1987), to be published in the proceedings of the XVth International Winter Meeting on Fundamental Physics, Sevilla, Spain, 1987; F. Barreiro, J. Sanchez-Gomez (eds.), World Scientific
5. W. Bartel et al. JADE Collab.: Z. Phys. C—Particles and Fields 33 (1986) 23
6. W. Braunschweig et al. TASSO Collaboration: Contributed paper to the 1987 Lepton-Photon Symposium, Hamburg
7. P. Ghez, G. Ingelman: Z. Phys. C—Particles and Fields 33 (1987) 465
8. B. Andersson, G. Gustafson, G. Ingelman, T. Sjöstrand: Phys. Rep. 97 (1983) 31
9. G. Ingelman: Phys. Scr. 33 (1986) 39
10. T. Sjöstrand: Phys. Lett. 142B (1984) 420
11. G. Ingelman: the Lund Monte Carlo for deep inelastic lepton-nucleon scattering—LEPTO version 5.2, DESY preprint in preparation
12. G. Ingelman: DESY 87–144 (1987), to be published in the proceedings of the XVth International Winter Meeting on Fundamental Physics, Sevilla, Spain, 1987; F. Barreiro, J. Sanchez-Gomez (eds.), World Scientific
13. E. Eichten, I. Hinchliffe, K. Lane, C. Quigg: Rev. Mod. Phys. 56 (1984) 579, ibid. 58 (1986) 1047
14. G. Altarelli, G. Martinelli: Phys. Lett. 76B (1978) 89
15. A. Méndez: Nucl. Phys. B145 (1978) 199; R. Peccei: R. Rückl, Nucl. Phys. B162 (1980) 125; Ch. Rumpf, G. Kramer, J. Willrodt: Z. Phys. C—Particles and Fields 7 (1981) 337
16. G. Altarelli, G. Parisi: Nucl. Phys. B126 (1977) 298
17. A.H. Mueller: Phys. Lett. 104B (1981) 161 B.I. Ermolaev, V.S. Fadin: JETP Lett. 33 (1981) 269 G. Marchesini, B.R. Webber: Nucl. Phys. B238 (1984) 1
18. A. Peterson et al. Mark II Collab.: SLAC-PUB-4290 (1987) P.N. Burrows: TASSO Collab., private comm.
19. M. Bengtsson, T. Sjöstrand: Nucl. Phys. B289 (1987) 810
20. T. Sjöstrand, M. Bengtsson: Comput. Phys. Commun. 43 (1987) 367 T. Sjöstrand: Comput. Phys. Commun. 39 (1986) 347
21. M. Bengtsson, T. Sjöstrand, M. van Zijl: Z. Phys. C—Particles and Fields 32 (1986) 67
22. H.-U. Bengtsson, T. Sjöstrand: Comput. Phys. Commun. 46 (1987) 43
23. M. Arneodo et al. EMC Collab. Z. Phys. C—Particles and Fields 36 (1987) 527
24. P.N. Burrows, G. Ingelman: Z. Phys. C—Particles and Fields 34 (1987) 91 and in Proceedings of the Workshop on Physics at Future Accelerators, La Thuile, Italy, vol. II, p. 369, CERN 87–07 (1987)
25. G. Marchesini, B.R. Webber, in: Proceedings of the Workshop on Physics at Future Accelerators, La Thuile, Italy, vol. II, p. 364, CERN 87–07 (1987)
26. J. Feltesse: talk at the workshop on Physics at HERA, Hamburg, Oct. 1987, to appear in the proceedings
27. See Proceedings of the study of an ep facility for Europe, Ed. U. Amaldi, DESY 79/48, pp. 391–394 (1979)
28. S. Bethke: Heidelberg Habilitation Thesis, LBL 50–208 (1987)
29. The ZEUS detector: Technical Proposal, March 1986
30. W.R. Nelson, H. Hirayama, DO Rogers: SLAC Report 265 (1985)
31. ZEUS Collaboration: unpublished